Systematizing Rotor-Based Morphable Unmanned Aerial-Aquatic Vehicles Design: From Theory to Prototype

Dongyue Huang, Xuchen Liu*, Minghao Dou and Ben M. Chen
Department of Mechanical and Automation Engineering, The Chinese University of Hong Kong, Shatin, N.T., Hong Kong

OCEANS 2024 - SINGAPORE | 979-8-3503-6207-7/24/$31.00 ©2024 IEEE | DOI: 10.1109/OCEANS51537.2024.10752602

***Abstract*—In this paper, we introduce a comprehensive workflow for the design of rotor-based morphable Unmanned Aerial-Aquatic Vehicles (UAAVs), drawing upon established design principles from fixed-wing aircraft engineering. A key feature of this workflow is the incorporation of Sequential Quadratic Programming (SQP) to regulate the spatial relationship between Center of Gravity (CoG) and Center of Buoyancy (CoB). This optimization enhances the underwater safety of UAAVs. By the field test of the constructed two prototypes, each representing a distinct type of morphable UAAV, the effectiveness of the proposed workflow is validated.**

I. Introduction

In the wake of rapid advancements across various manufacturing sectors, there has been a growing demand for vehicles capable of operating in multiple mediums, transcending the limitations of those confined to a single medium. Representative examples include Unmanned Aerial-Aquatic Vehicles (UAAVs) based on fixed-wing platforms (see [1]–[4]), conventional quadrotors (see [5], [6]), and hybrid wing systems (see [7]–[9]). These UAAVs offer tailored solutions to specific challenges inherent to their operational contexts. As expounded in this review [10], the disparate characteristics of different mediums necessitate modifications in the UAAVs' underwater configurations.

Morphable UAAVs are particularly advantageous in this regard, as they offer the flexibility to adapt to both aerial and aquatic environments, thereby enhancing their underwater efficacy. Regretfully, while there are existing prototypes of morphable UAAVs based on fixed-wing (see [11], [12]), these prototypes often sacrifice the maneuverability characteristics inherent to Remotely Operated Vehicles (ROVs) in underwater environments. In contrast, prototypes based on rotor are able to retain these maneuverability features.

Consequently, lots of researchers focus on the rotor-based morphable UAAV. Tan and Huang elaborate on the intricate details of the design, including motor selection methods that balance efficiency in both aquatic and aerial environments, waterproofing specifics, and the mechanical structures driving the rotation of the thrust plant (see [13]–[19]). Liu and Dou (see [20]–[22]), on the other hand, focuses on a particular inspection task and introduces a novel morphable UAAV with vector-tilting capabilities. They also incorporate a gearbox to optimize propulsion efficiency across different mediums. Rao's work [23], in contrast, emphasizes comprehensive testing in attitude control. These diverse approaches highlight the multifaceted challenges and solutions in the design and application of UAAVs, underscoring the need for a unified design methodology.

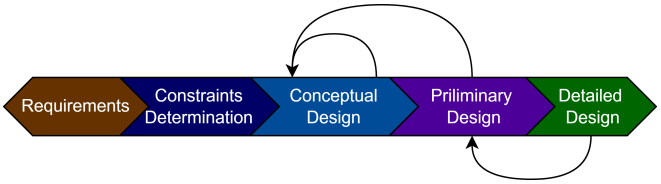

Fig. 1. Overview of design workflow for rotor-based morphable UAAVs.

Despite the proliferation of various rotor-based morphable UAAVs in contemporary research, there is a glaring absence of a unified design methodology. This lack of standardization not only undermines the effectiveness of the design but also hampers the field's further development. Unlike large fixed-wing aircraft, which have well-established design processes, UAAVs often resort to empirical methods and subsequent engineering adjustments.

Moreover, the unique requirements for underwater operation, specifically the relative positioning of the Center of Buoyancy (CoB) and the Center of Gravity (CoG), are often overlooked. It is well-known that the vehicle will achieve static stability if the CoG is located below the CoB, generating a restoring moment as illustrated in [24]. Conversely, if the CoG is above the CoB, the vehicle is prone to capsizing. However, many current designs overlook this crucial factor, generally relying on empirical methods or post-hoc engineering adjustments to address them, such as the addition of extra foam blocks, rather than utilizing the components of the vehicle itself. While additional buoyancy control modules in submersibles like ROVs can achieve similar goals, for UAAVs intended for aerial operations, the inclusion of extra components is impractical. This is despite the fact that Wang has previously explored the optimization of the CoG and CoB from a rigid body's fabrication standpoint in [25]. Therefore, there is an urgent need for a systematic design approach that explicitly incorporates these pivotal considerations.

To this end, we introduce a comprehensive design workflow tailored to the unique characteristics of rotor-based morphable UAAVs, drawing upon established design principles from fixed-wing aircraft. Furthermore, recognizing the critical role that the CoB and CoG play in the underwater performance of

the system, we incorporate a Sequential Quadratic Programming (SQP)-based optimization process into the workflow. This optimization aims to enhance the vehicle's performance from a mechanical design perspective. Finally, to validate the efficacy of the proposed design guidelines, we construct and evaluate two different prototypes, thereby confirming the rationality and effectiveness of our design workflow.

Contributions. 1) A design workflow, inspired by fixed-wing aircraft methodologies, is introduced to streamline the development process of rotor-based morphable UAAVs. 2) Sequential Quadratic Programming is integrated into the workflow to optimize the relative positions of the CoG and CoB, thereby ensuring both safety and mission-specific performance criteria are met. 3) The efficacy of the proposed workflow is validated through the design and evaluation of two distinct prototypes of morphable UAAVs.

II. Design Methodology

In Anderson's 1998 workflow for fixed-wing aircraft design, as depicted in [26], the core principle centers on fulfilling payload or specialized mission requirements. Utilizing existing models and prior knowledge, the workflow identifies a set of critical parameters, such as Lift-to-Drag ratio (L/D) and Wing Loading (W/S), to serve as constraints. Through iterative design, this methodology yields a more reliable aircraft while significantly reducing associated costs. This approach bears logical similarities to the design process for rotor-based morphable UAAVs. Consequently, it is advantageous to adapt Anderson's foundational principles to the unique characteristics of rotor-based morphable UAAVs, such as their variable morphology, in order to develop a specialized design workflow tailored specifically for these multifaceted platforms.

As illustrated in Fig. 1, the entire design workflow is segmented into five essential phases. The process begins with the Requirements phase, where a set of constraints is established based on specific operational needs. The design then advances through the Conceptual Design, Preliminary Design, and Detail Design phases, culminating in the actualization of the target vehicle. This structured approach guarantees a systematic and coherent progression from initial requirements to the final design.

A. Requirements and Constraints Determination

Before starting the main design process, it's important to clearly define constraints, like the estimated mass for each term, generated from these requirements, as illustrated as

$$\tilde{m} = \alpha(\tilde{m}_{\mathrm{e}} + \tilde{m}_{\mathrm{s}} + \tilde{m}_{\mathrm{b}} + \tilde{m}_{\mathrm{m}}), \tag{1}$$

where $\tilde{m}$ stands for the first estimated mass or maximum estimated mass, $\tilde{m}_{\mathrm{e}}$ stands for the estimated mass of the electronic, $\tilde{m}_{\mathrm{s}}$ stands for the initial guess mass of sealing components, $\tilde{m}_{\mathrm{b}}$ is the estimated battery mass, $\tilde{m}_{\mathrm{m}}$ is the initial guess of morphable components mass, and α is a first estimation coefficient.

Firstly, specifying mission requirements and scenarios for the UAAV should be considered. The design needs will vary depending on the vehicle's purpose. For example, a UAAV built for delivery might focus on carrying more weight and may use comparatively simpler sensors. On the other hand, a UAAV designed for exploration would likely require high-quality sensors, even if they are heavier. Consequently, an initial estimation of electronic can be ascertained.

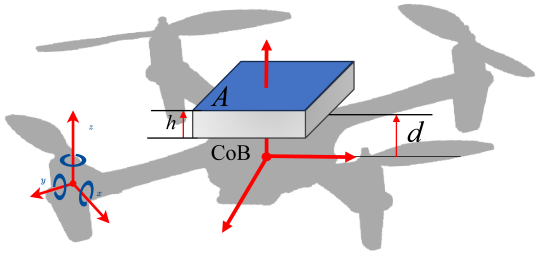

Fig. 2. Coordinate of propulsion unit and conceptual diagram with a hypothetical buoyancy cabin's distribution of a conventional quadrotor.

A second critical consideration is the operational depth at which the UAAV is intended to function. This parameter is of particular importance as the waterproofing components, including the main body and propulsion motors, often constitute a significant fraction of the vehicle's overall mass. The waterproofing techniques suitable for shallow operational depths, such as 10 meters, may differ substantially from those required for deeper deployments, such as 100 meters. Table I provides a comparative analysis of prevalent sealing methodologies employed in underwater robotics. Additionally, the type of fluid medium in which the UAAV will operate is also a crucial factor, especially when considering the potential for corrosive effects on motors and other components in saline environments.

The third pivotal consideration is the delineation of the vehicle's estimated endurance both in aquatic and aerial environments. The duration of operational endurance significantly influences the size of the battery required, which in turn has a substantial impact on the overall weight estimation of the vehicle. The final component to address is the morphing strategy, which is predominantly divided into two primary categories: body morphing and thrust direction morphing. The most prevalent approach in current designs involves altering the orientation of the thrust. As illustrated in the accompanying Fig. 2, this is achieved by rotating the thrust vector around x [27], or y [28], or z [29], to facilitate morphing. Consequently, it is worth noting that the weight of the core components driving this morphing will significantly impact the overall weight estimation of the vehicle. Finally, beyond the aforementioned parameters, it is necessary to specify the designed range of the wheelbase.

B. Conceptual Design

This section primarily focuses on the conceptual design stage, which aims to develop a conceptual model based on vague requirements and constraints. Conceptual design plays a crucial role in clarifying the overall direction and feasibility of the design, thereby providing clear guidance for subsequent

TABLE I
COMPARISON OF COMMON SEALING METHODS FOR UNDERWATER VEHICLES

Sealing Method	Advantages	Disadvantages
O-Ring Seals	Simple, cost-effective, easy to replace	Limited pressure and temperature range
Mechanical Seals	High-pressure, long-lasting	Complex, expensive
Gaskets	Simple, inexpensive	Limited conditions
Radial Shaft Seals	Effective for rotary applications	Wear over time
Face Seals	High-pressure and temperature	Complex, expensive
Labyrinth Seals	No contact, high-speed	Less effective at low speeds
Magnetic Fluid Seals	Wide range of pressures, no mechanical wear	Complex, expensive
Inflatable Seals	Conforms to shapes, variable gaps	Requires pressure source, potential failure
Compression Packing	Simple, inexpensive, easy to install	Requires maintenance
Welded Seals	Permanent, extreme conditions	Cannot be disassembled
Epoxy Seals	Simple, can be used with other methods	Permanent, difficult to remove

work. For the conceptual design of UAAVs, the process can be broadly divided into three main components: cabin allocation, morphing concept, and waterproofing strategy.

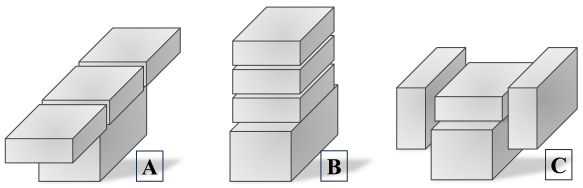

Fig. 3. Examples of cabin allocation concepts.

Firstly, in the design of UAAV cabins, we employ a commonly used approach in engineering design known as module design. This method involves modularizing the design based on the function of each cabin. For instance, the strong electrical power cabin that supports the power system is usually placed in a central location for easier wiring. Additionally, the overall shape of the vehicle, is also a consideration under cabins allocation, like elongated as shown in A of Fig. 3 or tower-like as shown in B of Fig. 3 or compact as shown in C of Fig. 3.

Secondly, based on the requirements defined in the previous section, this section delves into the specifics of how to achieve a morphable design. For example, the mechanical principles driving the morphing need to be considered in more detail. The morphable concept model derived from this part can effectively validate whether the chosen morphing strategy is appropriate.

Lastly, we consider the waterproofing strategy. Based on the sealing methods outlined in the previous section, we aim to design a suitable waterproof cabin strategy. Options include clip-on cabins, screw-threaded cabins, and screw-type cabins. Clip-on cabins offer the advantage of easy assembly and disassembly and allow for more flexible shaping compared to screw-threaded cabins, which are typically circular. Moreover, clip-on cabins can reduce the extra weight associated with waterproof components, unlike screw-type cabins that rely on the force applied by screws for sealing. However, clip-on cabins require careful consideration of material properties to achieve optimal waterproofing performance.

C. Preliminary Design

In the preliminary design phase, following the conceptual model, essential functionalities are integrated into the vehicle. The overall process of preliminary design, as shown in Fig. 4, generally consists of endow functionality, material selection, a secondary weight estimation, and the choice of an appropriate propulsion unit based on the re-estimated weight. Subsequently, the material strength limits are verified based on the power provided by the selected propulsion unit. Finally, the preliminary model is obtained by optimizing the positions of the CoG and the CoB.

In essence, the entire preliminary design process involves endowing the vehicle with functional capabilities. The endow functionality phase, as shown in Fig 4, as part of this process, specifically refers to the detailed implementation of features discussed in the conceptual model, including cabin allocation, the morphing concept, and waterproofing strategies. For instance, the morphing concept demands tailored solutions based on the selected approach, such as choosing gear sizes and other pertinent hardware to fulfill the design requirements.

For material selection, the choice is guided by the functional requirements of individual components and the overall mission objectives. For instance, high-strength materials like carbon fiber are typically chosen for structurally critical components. For waterproofing compartments, options range from UV-cured 3D-printed structures to injection-molded components that offer higher strength and are suitable for greater diving depths. After determining the materials for each component, a second-round weight estimate, denoted as $\tilde{m}_2$, is obtained based on the conceptual model and updated constraint parameters, illustrated as

$$\tilde{m}_2 = \tilde{m}_\mathrm{f} + \tilde{m}_\mathrm{e} + \tilde{m}_\mathrm{s} + \tilde{m}_\mathrm{b} + \tilde{m}_\mathrm{m}, \tag{2}$$

where $\tilde{m}_\mathrm{f}$ is the estimated framework mass.

As a rotor-based morphable UAAV, the core propulsion unit is comprised of motors, propellers, and electronic speed controllers (ESCs). The selection of this unit is inherently critical. Based on the second-round weight estimation, an aerial-compatible propulsion unit can be selected, which has an estimated mass $\tilde{m}_\mathrm{ppu}$, akin to conventional rotor-based UAVs. However, the unique challenge for UAAVs lies in satisfying power requirements for both aerial and aquatic environments.

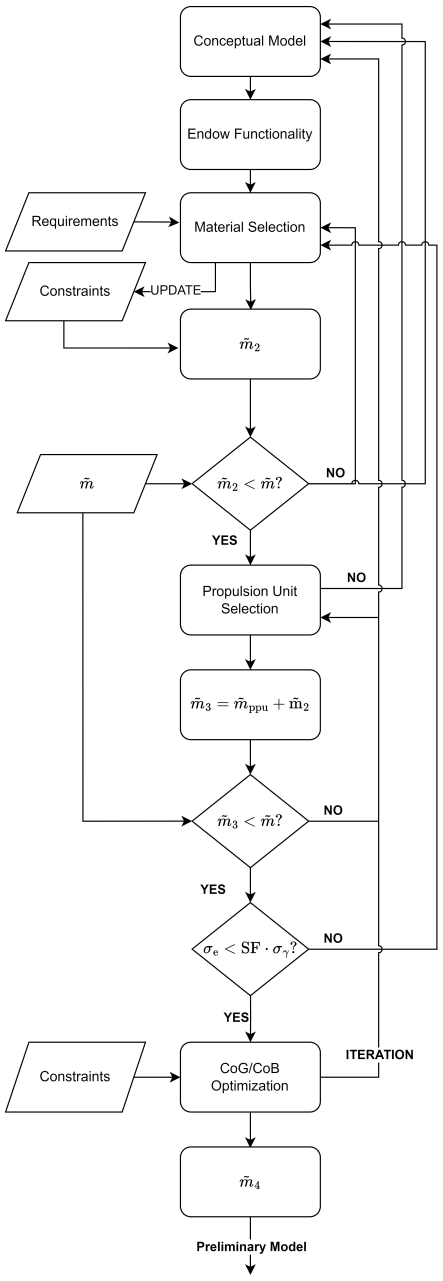

Fig. 4. Overall process of preliminary design.

Current strategies include: (A) employing separate propulsion systems for air and water in [30], (B) utilizing a trade-off approach to select a dual-purpose propulsion system in [15], or (C) augmenting the aerial propulsion system with a gearbox to meet underwater power requirements in [20]. Furthermore, after selecting an appropriate propulsion unit, it is essential to ensure that there is no interference between the morphing components and the various cabins of the main body. If interference is detected, cabin allocation must be re-evaluated.

Upon finalizing the aforementioned considerations, it is imperative to verify the concentrated stress of key load-bearing components, denoted as σ_{e}. This should be compared with the material's yield stress, denoted as σ_γ. Under the safety factor SF, it must be ensured that the component stress is less than the material's yield stress. If this condition is not met, material selection must be revisited.

D. CoG/CoB Optimization

For underwater motion, the relative positions of the CoG and the CoB are crucial for the vehicle's safety and maneuverability. In this section, we handle the optimization of these relative positions by a Sequential Quadratic Programming (SQP) algorithm.

Given that the majority of the vehicle's structure has already been determined in preliminary design with a random size of the buoyancy cabin, we assume that both the CoG and CoB are aligned along the z-axis of the body frame and the vehicle is fully submerged. The initial positions are denoted as $z_{\text{CoB},0}$ and $z_{\text{CoG},0}$, respectively. Also the initial displacement volume is denoted as $V_{\text{d},0}$. To facilitate the optimization, we introduce a hypothetical cabin, which is integral at a distance of d mm from the CoB of the original vehicle with a uniform density ρ of the material of it, referred to as the buoyancy cabin.

The hypothetical cabin conceptualized in this study is defined with a general framework, allowing the adoption of regular geometric shapes as per specific requirements, such as cylinders, hemispheres, rectangles, etc., as illustrated in the

Algorithm 1 SQP for Optimizing $z_{\text{CoB}} - z_{\text{CoG}}$

Initialize: Set initial guess h_0, tolerance ϵ, maximum iterations N, line search parameter γ, positive buoyancy tuning parameter $\mathcal{K}_{\text{opt}}$, and safety factor $\mathcal{K}_{\text{safe}}$.
Set: $k = 0$
while $k < N$ **do**
  Calculate gradient ∇f and Hessian H at h_k.
  Formulate the Quadratic Programming (QP) subproblem:

$$\begin{aligned} \max_{\Delta h} \quad & \frac{1}{2} H(h_k)(\Delta h)^2 + \nabla f(h_k)\Delta h \\ \text{s.t.} \quad & V_{\text{d,tot}} = V_{\text{d},0} + \Delta V_{\text{d}}(\Delta h) + V_{\text{d,k}}(h_k), \\ & V_{\text{s,tot}} = \Delta V_{\text{s}}(\Delta h) + V_{\text{s,k}}(h_k), \\ & V_{\text{d,tot}} \geq \frac{\mathcal{K}_{\text{opt}}}{\rho_{\text{w}}}(\tilde{m}_3 + \rho V_{\text{s,tot}}), \\ & V_{\text{s,tot}} \leq \frac{\mathcal{K}_{\text{safe}}(\tilde{m} - \tilde{m}_3)}{\rho}, \\ & |h| \leq |h_{\max}|. \end{aligned}$$

  Solve the QP subproblem to get Δh^*.
  Update $h_{k+1} = h_k + \gamma \Delta h^*$.
  if $|\Delta h^*| < \epsilon$ **and** change in objective function is small **then**
    break
  end if
  $k = k + 1$
end while
Output: Optimized $h^* = h_{k+1}$

Fig. 2. The position of the center of buoyancy is denoted as z_{B}, and the center of gravity is represented as z_{G} for the cabin. At a given height x, the external cross-sectional area of the cabin is defined as $A(x)$, while the internal cross-sectional area is denoted as $A_{\Delta}(x)$, with a wall thickness of d_{Δ} . With the total height of the cabin being h, which is the optimal parameter, the displaced volume V_{d} and the shell volume V_{s} can be mathematically expressed as:

$$V_{\mathrm{d}} = \int_0^h A(x)\mathrm{d}x, \tag{3}$$

$$V_{\mathrm{s}} = \int_0^h (A(x) - A_{\Delta}(x))\mathrm{d}x + \mathcal{H}(x)A(h)d_{\Delta}. \tag{4}$$

where

$$\mathcal{H}(x) = \begin{cases} 1, & \text{if } \mathrm{d}A(x)/\mathrm{d}x = 0, \ \ \forall x \in [0, h] \\ 0, & \text{otherwise} \end{cases} \tag{5}$$

By Archimedes' law, the object function, consisted of the difference between CoB and CoG of the vehicle after adding the buoyancy cabin can be illustrated as

$$f(h) = z_{\mathrm{CoB}} - z_{\mathrm{CoG}}, \tag{6}$$

with

$$z_{\mathrm{CoB}} = \frac{V_{\mathrm{d},0} \cdot z_{\mathrm{CoB},0} + V_{\mathrm{d}} \cdot z_{1\mathrm{B}}}{V_{\mathrm{d},0} + V_{\mathrm{d}}}. \tag{7}$$

$$z_{\mathrm{CoG}} = \frac{\tilde{m}_3 \cdot z_{\mathrm{CoG},0} + \rho V_{\mathrm{s}} \cdot z_{1\mathrm{G}}}{\tilde{m}_3 + \rho V_{\mathrm{s}}}, \tag{8}$$

where $z_{1\mathrm{B}} = d + z_{\mathrm{B}} + z_{\mathrm{CoB},0}$ and $z_{1\mathrm{G}} = d + z_{\mathrm{G}} + z_{\mathrm{CoB},0}$ represent the position of CoB and CoG of cabin from the CoB of the origin body respectively.

Then, as illustrated in Algorithm 1, (7), and (8), we employ SQP to optimize the relative positions of the CoB and the CoG during design. The objective is to maximize the distance between them, subject to constraints on the vehicle's mass, among other factors. The SQP algorithm iteratively refines the solution by solving a series of Quadratic Programming (QP) subproblems. In each iteration, the nonlinear objective function and the constraints are linearized around the current estimate. The resulting QP subproblem is then solved to obtain an updated direction for the decision variable h. The algorithm operates in an iterative manner. In each iteration, it updates the estimates for z_{CoB} and z_{CoG}. It then resolves the QP subproblem and the process continues until the changes in both the objective function and constraints are below a predefined tolerance level. This approach allows us to efficiently navigate the design space while ensuring that the final design meets the specified constraints.

E. Detailed Design

In the context of detailed design, the primary focus lies in refining specific elements. For instance, based on the preliminary model, designs for manufacturing and assembly are created, complete with tolerances. This is essential as components requiring assembly must account for material tolerances that arise during the manufacturing process. Additionally, the design phase also involves the selection of necessary hardware such as screws and bolts. Finally, if there are additional task-specific requirements, these can be integrated into this stage of the design process. The final estimation mass can be explained as

$$\tilde{m}_5 = \beta(\tilde{m}_4 + \tilde{m}_{\delta}), \tag{9}$$

where β is the final estimation coefficient, used for estimating the mass of the fasteners components, usually ranging from 1.05 to 1.1, $\tilde{m}_{\delta}$ is the mass from the other supplements.

III. Prototypes Construction

In this section, we present two distinct prototypes from a systematic design perspective, focusing on the logical framework of the design process and optimization of CoB and CoG. For more detailed design aspects, please refer to [13] and [20]. The first set is referred to as the Coupling Tiltable UAAV, and the second set is called the Vectorial Tiltable UAAV. The key distinction between the two lies in the control of thrust directions: in the Coupling Tiltable UAAV, the thrust directions change collectively, whereas in the Vectorial Tiltable UAAV, they are adjusted individually.

A. Coupling Tiltable UAAV

For the Coupling Tiltable UAAV, as the name suggests, its morphing strategy synchronizes the tilting of all thrust directions. This approach intuitively allows for a reduction in the number of servo motors, leading to a lighter and more compact vehicle. As a result, it is well-suited for large-scale swarm operations, such as serving as communication relays or array nodes.

In line with these task requirements and inspired by Tan's primary design in [16], we redesigned a lightweight and compact prototype for validating the design method, named Mirs-Alioth.

At the initial guess, the electronic, we focused on a flight controller, four ESCs, a battery elimination circuit (BEC) and a power distribution board (PDB), with approximate weights m_{e} as 140 g and m_{b} as 120 g for the estimated battery mass. As for sealing components, given that the operational depth is approximately 1-2 meters underwater, the waterproofing requirements are not stringent. We thus opted for a gasket-based solution. Sealing components weight estimates as 15 g, and the servo motors for driving the morphing mechanism add another 45 g. With a first estimated parameter $\alpha = 2.5$, we can complete the initial constrained design and get the maximum estimated mass 800 g, as shown in the initial guess of Table II.

In the conceptual design phase, we adopted the cabin arrangement depicted in part C of Fig. 3, as inspired by the principles outlined in [14]. This approach offers the advantage of ensuring a compact core while utilizing the surrounding lateral compartments to house lightweight electronic components and facilitate buoyancy adjustment. As the prior knowledge provided by Tan's work, to facilitate easier assembly and disassembly for initial testing, we continued to incorporate multiple

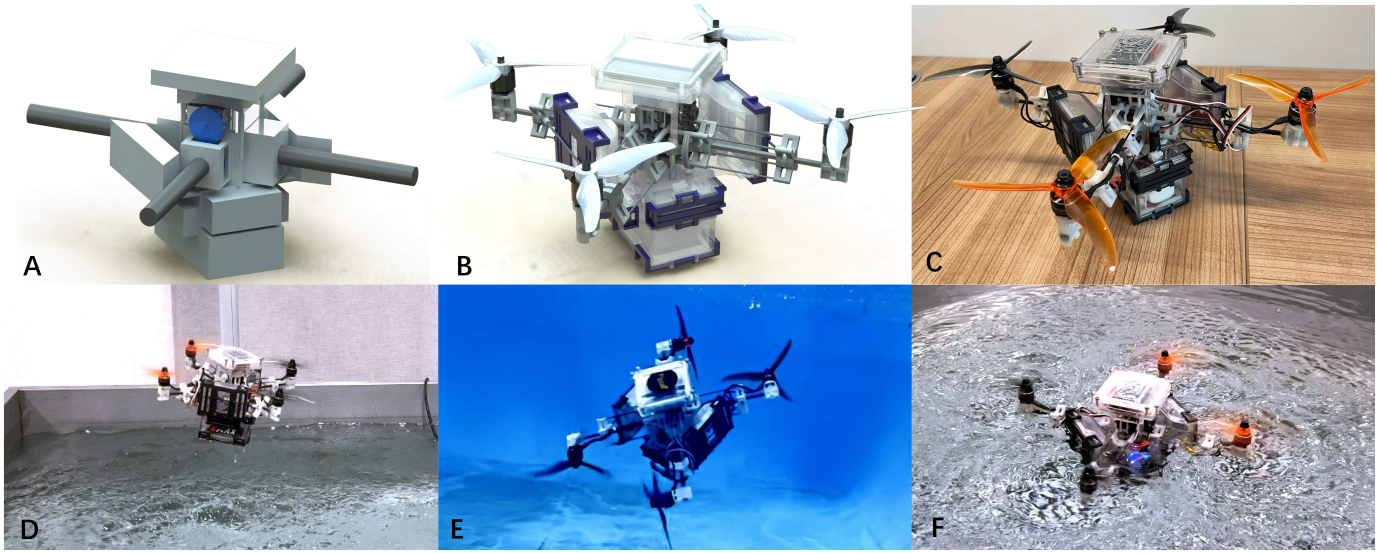

Fig. 5. Snapshots of Mirs-Alioth during the iteration and the field test, (A) is the model from conceptual design, (B) is the model after the CoB/CoG optimization of the preliminary design, (C) is the prototype, from (D) to (F) are the snapshots of the field test in the air, underwater, and in the transition respectively.

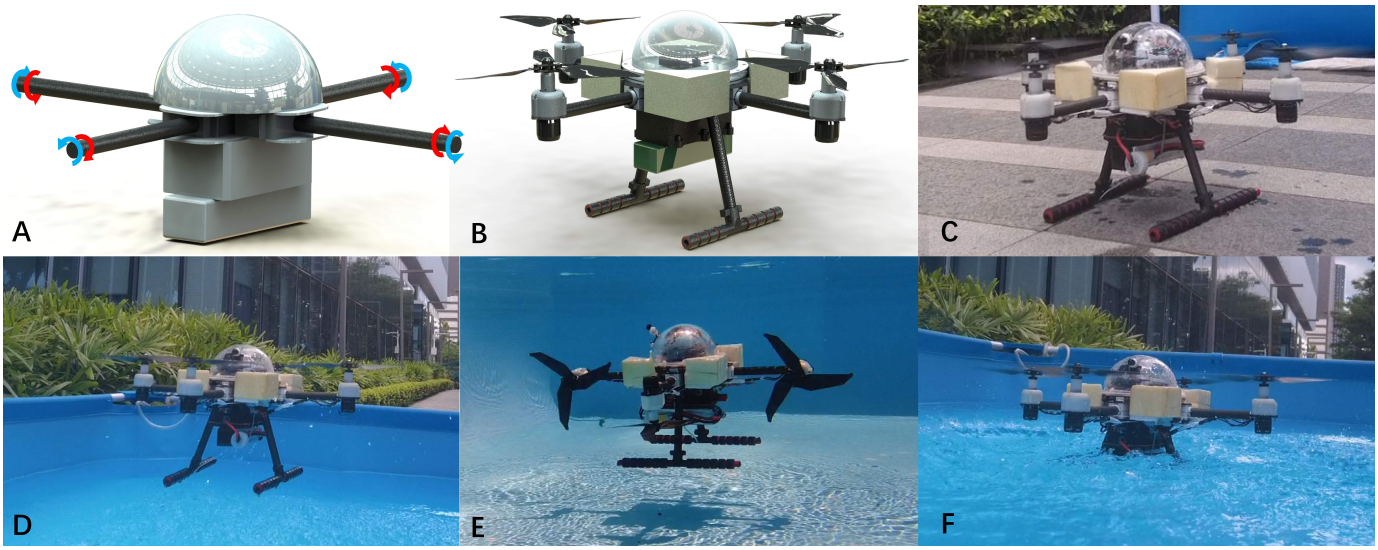

Fig. 6. Snapshots of Mirs-Cross during the iteration and the field test, (A) is the model from conceptual design, (B) is the model after the CoB/CoG optimization of the preliminary design, (C) is the prototype, from (D) to (F) are the snapshots of the field test in the air, underwater, and in the transition respectively.

openings and employed snap-fit structures for waterproofing. And we implemented the symmetrically synchronized tilting by using four bevel gears driven by a servo motor, as shown in Fig. 7, as proposed by Tan in [16]. Eventually, a conceptual model is constructed as shown in Fig. 5A.

In the material selection section, we chose to 3D-print the hull as a monolithic structure, which includes the buoyancy cabin for subsequent optimization. The material selected is SOMOS® WATERCLEAR ULTRA 10122, chosen for its unique combination of strength and elasticity. Additionally, the arm structure follows the design in the referenced literature, using a combination of photopolymer material SOMOS® GP+ and carbon fiber rods to form an exoskeleton, thereby reducing weight. SOMOS® LEDO is used as the primary material for the clip-on components. As shown in Table II for more details, an initial height of cabin h_0 is determined as 30 mm and d is determined as -10 mm , with $\mathcal{K}_{\text{opt}}$ and $\mathcal{K}_{\text{safe}}$ as 1.2 and 0.78 in the Algorithm 1. Eventually, with the height of the cabin h converge to 50.51 mm, as shown in Fig. 8, a preliminary model can be constructed as shown in Fig. 5B. Moreover, two main changes occur during this optimization. Firstly, from Table II, the displacement volume V rises up to 6.882×10^4 mm^3, implying that buoyancy force overtakes the gravity after optimization. Secondly, the distance between CoB and CoG

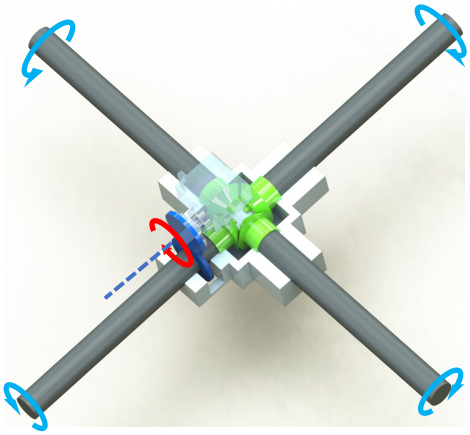

Fig. 7. Concept of morphing method.

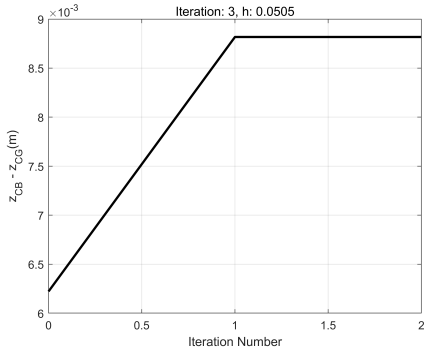

Fig. 8. Distance between CoB/CoG during the iteration of Mirs-Alioth

increasing to 8.818 mm, showing a better underwater static stability.

By choosing the final estimation parameter β as 1.1 for estimating the mass of fasteners like screws and cables, the weight of the model obtained through the design process was finalized as 706.41 g. As illustrated in Fig. 5C and last column of Table II, the mass of the prototype is 700.27 g and the displacement volume is 7.026×10^4 mm^3. Moreover, the distance between CoB and CoG is 8.340 mm, which is close to the estimation value after the optimization, and is bigger than the initial value before the optimization. Except that, a series of field tests are conducted on the prototype as shown from D to E in Fig. 5, showing that the proposed design methodology ensures that the set of features and requirements envisioned at the beginning of the design process are realized.

B. Vectorial Tiltable UAAV

The Vectorial Tiltable UAAV, as the name suggests, is able to have vectorial thrust tilting, which frees it from many of the limitations of under-actuated systems and allows it to generate more complex motions for different oceanographic applications. Then by the proposed design method, a vectorial tiltable UAAV was designed, named Mirs-Cross.

At the initial estimation stage, the mass of the electronic devices $\tilde{m}_\mathrm{e}$ is approximated to be about 400 g. This encompasses a flight controller, a PDB, a 4-in-1 ESC, a MOS Field-Effect Transistor (MOSFET), two BECs, a depth gauge, and a control knob. The mass of the battery $\tilde{m}_\mathrm{b}$ is estimated at 370 g. Considering the operational depth, which ranges from 2 to 4 meters, the primary sealing method employed is an o-ring based system, complemented by epoxy seals as a secondary measure. Consequently, the estimated sealing mass $\tilde{m}_\mathrm{s}$ is around 30 g. Additionally, considering that rotor-based UAAVs require at least two additional inputs, in addition to their four primary ones, to achieve fully or over-actuation, 2 to 4 servo motors are then utilized. This arrangement leads to a maximum estimated mass for the morphing components $\tilde{m}_\mathrm{m}$ of 200 g. Adopting a estimation coefficient α of 2.3, the maximum estimated total mass $\tilde{m}$ is calculated to be 2300 g.

Following that, as depicted in Fig. 3, we opted for Strategy B for our cabin allocation. This choice was driven by our preference to arrange the high-power and low-power cabins separately, allocating the intermediate space for morphing components. Moreover, we adopted a screw-type waterproofing strategy combined with an o-ring based sealing method for the overall waterproof design for desired submersion depth. Lastly, to facilitate individual tilting of each arm and avoid complexities associated with intricate mechanical structures, we chose the most straightforward yet effective solution: using four separate servos to drive each arm, as shown in Fig. 6A.

As depicted in column "Before Optimization" in Table III and Fig. 4, we outline the estimated parameters in our preliminary design before optimization, emphasizing several key aspects. Firstly, concerning material selection, Poly(methyl methacrylate) (PMMA) is chosen for the upper hemispherical structure due to its transparency, enhancing internal device visibility. The lower section, housing the power system, will utilize injection molding to reinforce seal strength and ensure waterproofing. Core structural components, including the vehicle's arms and main body, will be crafted from carbon fiber, optimizing structural integrity and weight efficiency. The servo motor mounts, less demanding in strength, are to be 3D printed using SOMOS® GP+. Secondly, in contrast to Mirs-Alioth, this vehicle, albeit less complex in function morphing, incorporates a sophisticated gearbox in the propulsion unit to improve efficiency in both underwater and aerial modes. For further details on these design aspects, refer to [20]. Lastly, CoG and CoB are almost overlapped and the vehicle is negative buoyancy, which is unsatisfactory to the requirements.

Upon selecting $\mathcal{K}_\mathrm{opt}$ and $\mathcal{K}_\mathrm{safe}$ as 1.2 and 0.82 and integrating d as 55 mm , the Table III clearly shows two notable enhancements in the 'After Optimization' column under the mass constraint. First, there is an increase in the vehicle's displacement volume to 2.300×10^5 mm^3 , indicating positive buoyancy. Second, the distance between CoB and the CoG has risen from 0.6 to 16.957, as illustrated in Fig 9. During this optimization process, the radius of the upper buoyancy cabin, which also serves as the electronic enclosure, has been increased from an initial 50 mm to 70 mm.

An important point to note in the detail design phase is the addition of foam blocks located at the vehicle's shoulders,

TABLE II
VALUE'S CHANGES OF MIRS-ALIOTH'S PARAMETERS DURING THE DESIGN ITERATION

	Initial Guess	Before Optimization (i=3)	After Optimization (i=4)	Detailed Design (i=5)	Prototype
$\tilde{m}_{\text{opt}}$ (g)	-	-	23.85	-	-
$\tilde{m}_{\text{f}}$ (g)	-	244.34	244.34	-	-
$\tilde{m}_{\text{e}}$ (g)	140	140	140	-	-
$\tilde{m}_{\text{b}}$ (g)	120	120	120	-	-
$\tilde{m}_{\text{m}}$(g)	45	24	24	-	-
$\tilde{m}_{\text{s}}$(g)	15	14	14	-	-
$\tilde{m}_{\text{ppu}}$ (g)	-	76	76	-	-
$\tilde{m}_{\delta}$ (g)	-	-	-	-	-
$\tilde{m}_{i}$ (g)	800	618.34 ✓	642.19 ✓	706.41 ✓	700.27
V (mm^3)	-	5.744×10^4	6.882×10^4 ↑	-	7.026×10^4
CoG (mm)	-	-6.2	-4.006	-	-
CoB (mm)	-	0	4.812	-	-
CoB − CoG (mm)	-	6.2	8.818 ↑	-	8.340

TABLE III
VALUE'S CHANGES OF MIRS-CROSS'S PARAMETERS DURING THE DESIGN ITERATION

	Initial Guess	Before Optimization (i=3)	After Optimization (i=4)	Detailed Design (i=5)	Prototype
$\tilde{m}_{\text{opt}}$ (g)	-	-	177.40	177.40	-
$\tilde{m}_{\text{f}}$ (g)	-	753.97	753.97	-	-
$\tilde{m}_{\text{e}}$ (g)	400	400	400	-	-
$\tilde{m}_{\text{b}}$ (g)	370	370	370	-	-
$\tilde{m}_{\text{m}}$(g)	200	176.11	176.11	-	-
$\tilde{m}_{\text{s}}$(g)	30	19.24	19.24	-	-
$\tilde{m}_{\text{ppu}}$ (g)	-	248.20	248.20	-	-
$\tilde{m}_{\delta}$ (g)	-	-	-	11.2	-
$\tilde{m}_{i}$ (g)	2300	1967.15 ✓	2144.60 ✓	2264.02✓	2237.76
V (mm^3)	-	1.875×10^5	2.300×10^5 ↑	2.900×10^5	3.080×10^5
CoG (mm)	-	-0.6	0.958	15.505	-
CoB (mm)	-	0	17.915	38.477	-
CoB − CoG (mm)	-	0.6	16.957 ↑	22.971	21.083

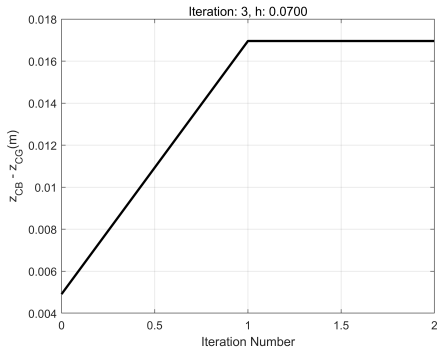

Fig. 9. Distance between CoB/CoG during the iteration of Mirs-Cross

as shown in Fig. 6B. The objective of this modification is to ensure that the propellers protrude above the water surface when the vehicle is afloat, facilitating easier take-off. However, this aspect falls outside the scope of the optimization algorithm proposed, as it involves dynamic changes in the positions of the CoB and CoG when part of the vehicle emerges above the water surface. The final model derived from the detailed design weighs 2155.8 g, with a distance of 22.971 mm between the center of buoyancy and gravity. Compared to the manufactured prototype, as shown in Fig. 6C, and the field test of prototype as shown from Fig. 6D to Fig. 6F, with a final weight of 2207.76 g, a displacement volume of 3.080×10^5 mm^3, and a CoB/CoG distance of 21.083 mm, it is evident that the design process effectively controls the overall mass, displacement volume, and CoB/CoG distance variations, demonstrating the reliability of the proposed design methodology.

IV. CONCLUSION

In this paper, we have developed a design process for rotor-based morphable UAAVs, drawing inspiration from fixed-wing aircraft design principles. We have enriched the details of this process by reviewing existing designs of rotor-based morphable UAAVs. Furthermore, by establishing a model for the vehicle's CoB and CoG, and optimizing their positions using SQP, we have validated the reliability and universality of our proposed process. This validation is exemplified through the design and analysis of two distinct UAAV prototypes. Despite these successful cases, more design examples are required to continue validating and refining our design process, aiming to enhance its application in practical marine exploration and scientific research.

REFERENCES

[1] D. Edwards, N. Arnold, S. Heinzen, C. Strem, and T. Young, "Flying emplacement of an underwater glider," in *OCEANS 2017-Anchorage*. IEEE, 2017, pp. 1–6.

[2] J. Moore, A. Fein, and W. Setzler, "Design and analysis of a fixed-wing unmanned aerial-aquatic vehicle," in *2018 IEEE International Conference on Robotics and Automation (ICRA)*, 2018, pp. 1236–1243.

[3] T. Wang, X. Yang, J. Liang, G. Yao, and W. Zhao, "Cfd based investigation on the impact acceleration when a gannet impacts with water during plunge diving," *Bioinspiration & biomimetics*, vol. 8, no. 3, p. 036006, 2013.

[4] W. Weisler, W. Stewart, M. B. Anderson, K. J. Peters, A. Gopalarathnam, and M. Bryant, "Testing and characterization of a fixed wing cross-domain unmanned vehicle operating in aerial and underwater environments," *IEEE Journal of Oceanic Engineering*, vol. 43, no. 4, pp. 969–982, 2018.

[5] B. P. McNelly, R. L. Hooks, W. R. Setzler, and C. S. Hughes, "Additive manufacturing of pressure vessels (with plating)," in *Pressure Vessels and Piping Conference*, vol. 57946. American Society of Mechanical Engineers, 2017, p. V03AT03A025.

[6] N. Kaja and O. Akinsanya, "Evaluation of a quad-rotor powerplant for dual-mode (air and underwater) operation," 2014.

[7] D. Lu, C. Xiong, H. Zhou, C. Lyu, R. Hu, C. Yu, Z. Zeng, and L. Lian, "Design, fabrication, and characterization of a multimodal hybrid aerial underwater vehicle," *Ocean Engineering*, vol. 219, p. 108324, 2021. [Online]. Available: https://www.sciencedirect.com/science/article/pii/S0029801820312373

[8] D. Lu, C. Xiong, Z. Zeng, and L. Lian, "Adaptive Dynamic Surface Control for a Hybrid Aerial Underwater Vehicle with Parametric Dynamics and Uncertainties," *IEEE Journal of Oceanic Engineering*, vol. 45, no. 3, pp. 740–758, 2020.

[9] C. Lyu, D. Lu, C. Xiong, R. Hu, Y. Jin, J. Wang, Z. Zeng, and L. Lian, "Toward a gliding hybrid aerial underwater vehicle: Design, fabrication, and experiments," *Journal of Field Robotics*, vol. 39, no. 5, pp. 543–556, 2022.

[10] Z. Zeng, C. Lyu, Y. Bi, Y. Jin, D. Lu, and L. Lian, "Review of hybrid aerial underwater vehicle: Cross-domain mobility and transitions control," *Ocean Engineering*, vol. 248, p. 110840, 2022.

[11] W. Stewart, W. Weisler, M. MacLeod, T. Powers, A. Defreitas, R. Gritter, M. Anderson, K. Peters, A. Gopalarathnam, and M. Bryant, "Design and demonstration of a seabird-inspired fixed-wing hybrid uav-uuv system," *Bioinspiration & biomimetics*, vol. 13, no. 5, p. 056013, 2018.

[12] F. M. Rockenbauer, S. Jeger, L. Beltran, M. Berger, M. Harms, N. Kaufmann, M. Rauch, M. Reinders, N. R. Lawrance, T. Stastny *et al.*, "Dipper: A dynamically transitioning aerial-aquatic unmanned vehicle." in *Robotics: Science and Systems*, 2021, pp. 12–16.

[13] Y. H. Tan and B. M. Chen, "Underwater stability of a morphable aerial-aquatic quadrotor with variable thruster angles," in *2021 IEEE International Conference on Robotics and Automation (ICRA)*. IEEE, 2021, pp. 314–320.

[14] ——, "A morphable aerial-aquatic quadrotor with coupled symmetric thrust vectoring," in *2020 IEEE International Conference on Robotics and Automation (ICRA)*. IEEE, 2020, pp. 2223–2229.

[15] ——, "Thruster allocation and mapping of aerial and aquatic modes for a morphable multimodal quadrotor," *IEEE/ASME Transactions on Mechatronics*, vol. 25, no. 4, pp. 2065–2074, 2020.

[16] ——, "Design of a morphable multirotor aerial-aquatic vehicle," in *OCEANS 2019 MTS/IEEE SEATTLE*. IEEE, 2019, pp. 1–8.

[17] ——, "Motor-propeller matching of aerial propulsion systems for direct aerial-aquatic operation," in *2019 IEEE/RSJ International Conference on Intelligent Robots and Systems (IROS)*. IEEE, 2019, pp. 1963–1970.

[18] ——, "Survey on the development of aerial-aquatic hybrid vehicles," *Unmanned Systems*, vol. 9, no. 3, pp. 263–282, 2021.

[19] D. Huang, C. Wang, M. Dou, X. Liu, Z. Liu, B. Wang, and B. M. Chen, "Underwater motions analysis and control of a coupling-tiltable unmanned aerial-aquatic quadrotor," *arXiv preprint arXiv:2312.07290*, 2023.

[20] X. Liu, M. Dou, D. Huang, B. Wang, J. Cui, Q. Ren, L. Dou, Z. Gao, J. Chen, and B. M. Chen, "Tj-flyingfish: Design and implementation of an aerial-aquatic quadrotor with tiltable propulsion units," in *2023 IEEE International Conference on Robotics and Automation (ICRA)*, 2023.

[21] X. Liu, M. Dou, R. Yan, D. Huang, S. Gao, B. Wang, J. Cui, Q. Ren, L. Dou, Z. Gao, J. Chen, and B. M. Chen, "Tj–flyingfish: An unmanned morphable aerial–aquatic vehicle system," *Unmanned Systems*, 2023.

[22] M. Dou, X. Liu, D. Huang, B. Wang, J. Cui, Q. Ren, L. Dou, J. Chen, and B. M. Chen, "Modeling and operating point analysis for aquatic translational motion of a cross-medium vehicle," in *2023 42nd Chinese Control Conference (CCC)*, 2023, pp. 1351–1357.

[23] H. Rao, L. Xie, J. Yang, Y. Xu, W. Lv, Z. Zheng, Y. Deng, and H. Guo, "Puffin platform: A morphable unmanned aerial/underwater vehicle with eight propellers," *IEEE Transactions on Industrial Electronics*, 2023.

[24] T. I. Fossen, *Handbook of marine craft hydrodynamics and motion control*. John Wiley & Sons, 2011.

[25] L. Wang and E. Whiting, "Buoyancy optimization for computational fabrication," in *Computer Graphics Forum*, vol. 35, no. 2. Wiley Online Library, 2016, pp. 49–58.

[26] J. D. Anderson, "Aircraft performance and design," 1999.

[27] M. Ryll, H. H. Bülthoff, and P. R. Giordano, "Modeling and control of a quadrotor uav with tilting propellers," in *2012 IEEE international conference on robotics and automation*. IEEE, 2012, pp. 4606–4613.

[28] J. Shu and P. Chirarattananon, "A quadrotor with an origami-inspired protective mechanism," *IEEE Robotics and Automation Letters*, vol. 4, no. 4, pp. 3820–3827, 2019.

[29] S. Mintchev, L. Daler, G. L'Eplattenier, L. Saint-Raymond, and D. Floreano, "Foldable and self-deployable pocket sized quadrotor," in *2015 IEEE International Conference on Robotics and Automation (ICRA)*. IEEE, 2015, pp. 2190–2195.

[30] Y. Bi, Y. Jin, C. Lyu, Z. Zeng, and L. Lian, "Nezha-mini: Design and locomotion of a miniature low-cost hybrid aerial underwater vehicle," *IEEE Robotics and Automation Letters*, vol. 7, no. 3, pp. 6669–6676, 2022.